UNIVERSITY OF BIRMINGHAM
University of Birmingham Research at Birmingham

# Aerodynamic forces on generic buildings subject to transient, downburst-type winds

Jesson, Michael; Sterling, Mark; Letchford, Chris; Haines, Matthew

*DOI:*
10.1016/j.jweia.2014.12.003

*License:*
Creative Commons: Attribution (CC BY)

*Document Version*
Publisher's PDF, also known as Version of record

*Citation for published version (Harvard):*
Jesson, M, Sterling, M, Letchford, C & Haines, M 2015, 'Aerodynamic forces on generic buildings subject to transient, downburst-type winds', *Journal of Wind Engineering and Industrial Aerodynamics*, vol. 137, pp. 58-68. https://doi.org/10.1016/j.jweia.2014.12.003

Link to publication on Research at Birmingham portal

**Publisher Rights Statement:**
Eligible for repository under Creative Commons License

Checked January 2015

**General rights**
Unless a licence is specified above, all rights (including copyright and moral rights) in this document are retained by the authors and/or the copyright holders. The express permission of the copyright holder must be obtained for any use of this material other than for purposes permitted by law.

•Users may freely distribute the URL that is used to identify this publication.
•Users may download and/or print one copy of the publication from the University of Birmingham research portal for the purpose of private study or non-commercial research.
•User may use extracts from the document in line with the concept of 'fair dealing' under the Copyright, Designs and Patents Act 1988 (?)
•Users may not further distribute the material nor use it for the purposes of commercial gain.

Where a licence is displayed above, please note the terms and conditions of the licence govern your use of this document.

When citing, please reference the published version.

**Take down policy**
While the University of Birmingham exercises care and attention in making items available there are rare occasions when an item has been uploaded in error or has been deemed to be commercially or otherwise sensitive.

If you believe that this is the case for this document, please contact UBIRA@lists.bham.ac.uk providing details and we will remove access to the work immediately and investigate.

Download date: 09. Apr. 2024

J. Wind Eng. Ind. Aerodyn. 137 (2015) 58–68

Contents lists available at ScienceDirect

Journal of Wind Engineering and Industrial Aerodynamics

journal homepage: www.elsevier.com/locate/jweia

# Aerodynamic forces on generic buildings subject to transient, downburst-type winds

Michael Jesson [a,*], Mark Sterling [a], Chris Letchford [b], Matthew Haines [a]

[a] School of Civil Engineering, University of Birmingham, Birmingham, UK
[b] School of Civil and Environmental Engineering, Rensselaer Polytechnic Institute, New York, USA

ARTICLE INFO

*Article history:*
Received 7 April 2014
Received in revised form
4 December 2014
Accepted 6 December 2014

*Keywords:*
Thunderstorm downbursts
Transient winds
Wind-structure interaction
Physical simulation
Impinging jets
Wind tunnel

ABSTRACT

Having been identified as the cause of design load winds in many parts of the world, transient winds such as gust fronts and thunderstorm downbursts have been increasingly researched over recent years. The difficulties in simulating the flow structure of downbursts in the laboratory, particularly their rapid radial acceleration and associated ring vortices, have complicated measuring wind loads on structures subject to these conditions. The University of Birmingham Transient Wind Simulator (UoB-TWS, a 1 m diameter impinging jet with aperture control) has been used to simulate the transient aspects of downburst-like flow, allowing the pressure distributions they create over cube and portal framed structures to be measured for the first time, at model-scale (1:1600). Analysis of the velocity and pressure fields show that the simulator is capable of creating velocity fields which are similar to those observed in nature. Development of the ring vortex is demonstrated through phase-plot analysis. Two methods of calculating the turbulence intensity of the unsteady flow field have been used, giving mean values of between 3% and 10% depending on the method. Force coefficient time series have been estimated with the buildings angled at 0°, 45° and 90° to the radial wind direction. These are presented along with the instantaneous pressure coefficient distribution at the time of maximum roof suction. This novel research also highlights the difficulties of undertaking transient flow at model scale and drawing conclusions which are applicable to full-scale, i.e., where no two events are the same.

© 2014 The Authors. Published by Elsevier Ltd. This is an open access article under the CC BY license (http://creativecommons.org/licenses/by/3.0/).

## 1. Introduction

Over the last few years there has been renewed interest in evaluating the impact of transient winds caused by convection in thunderstorm cells, i.e. gust fronts, downbursts and tornadoes. This has been driven by the acknowledgement that in many parts of the world it is such transient winds (rather than synoptic, boundary layer winds) which are the cause of design wind speeds (Chay and Letchford, 2002a). Research has been undertaken to physically simulate tornadoes (e.g. Chang, 1971; Haan et al., 2008; Jischke and Light, 1983; Mishra et al., 2008) and downbursts. The latter, which are the main subject of this paper, have been simulated in a number of ways: very small-scale density driven flows (e.g. Lundgren et al., 1992); slot jets (e.g. Butler and Kareem, 2007; Lin et al., 2007); multi-fan wind tunnels (e.g. Butler et al., 2010); steady impinging jets (e.g. Chay and Letchford, 2002a,b; Choi, 2004; Wood et al., 2001; Zhang et al., 2013) and pulsed impinging jets (e.g. Haines et al., 2013; Mason, 2003; Mason et al., 2009a; McConville et al., 2009). Complementary research has been undertaken in terms of numerical simulation of downbursts (e.g. Butler and Kareem, 2007; Chay et al., 2006; Kim and Hangan, 2007; Mason, 2003; Mason et al., 2009b). In many of these studies, the emphasis has been on re-creating the familiar "nose" of a downburst outflow, in which the maximum horizontal streamwise velocity is seen to occur close to the ground, unlike the monotonically increasing, logarithmic distribution of atmospheric boundary layer (ABL) winds.

The pressure field on structures subject to downburst winds have been investigated in a number of the works mentioned above. Chay and Letchford (2002a) and Sengupta et al. (2008) measured pressure distributions over a cube exposed to a steady, translating, impinging jet at a relatively small scale (jet diameter $D=0.51$ m, $D=0.20$ m, $D=0.20$ m respectively). Mason et al. (2009a) attempted to simulate the ring vortex of a downburst using a pulsed version of Chay and Letchford's impinging jet, while Butler et al. (2010) examined the pressures on prismatic buildings in a 2-D downburst simulator. Butler et al. investigated the effects of varying the building height with respect to the height of the maximum outflow velocity. Zhang et al. (2013) examined the forces acting on gable-ended (portal) buildings under steady-state, impinging jet flow, with two roof angles examined. The above work have tended to express the

* Corresponding author. Tel.: +44 121 414 5065.
*E-mail address:* m.a.jesson@bham.ac.uk (M. Jesson).

http://dx.doi.org/10.1016/j.jweia.2014.12.003
0167-6105/© 2014 The Authors. Published by Elsevier Ltd. This is an open access article under the CC BY license (http://creativecommons.org/licenses/by/3.0/).

pressure and force data in terms of a generalised coefficients ($C_p$) and drag coefficients ($C_d$), defined as

$$C_p = \frac{p - p_{ref}}{\frac{1}{2}\rho V^2} \tag{1}$$

$$C_d = \frac{1}{A_s}\int_{A_s} C_p \, dA \tag{2}$$

where $p$ is the absolute pressure, $p_{ref}$ is a reference pressure, $\rho$ is the air density, $A_s$ is the total area of the surface under consideration, and $V$ is the velocity used to calculate a reference dynamic pressure for normalisation. When considering "closed" or sealed buildings, with negligible permeability, the internal pressure will tend to remain constant over the short duration of a transient wind event, and as such the static (atmospheric) pressure ($p_{atm}$) may be used for $p_{ref}$. For porous buildings where the internal pressure follows closely changes in the local static pressure which occur during the event, a reference pressure is more problematic and the local time varying static (atmospheric) pressure could be used when calculating forces. The choice of $V$ varies by application – for ABL winds, the eaves height wind-speed is the standard for normalisation (see, for example, Richards et al., 2001), and is the maximum wind-speed to which the windward surface is exposed; for transient flows the choice is complicated by spatial (varying vertical velocity profile) and temporal (transient nature of the flow) considerations. Full-scale data indicate that the maximum velocity occurs at a height $30\ \text{m} < z_m < 100\ \text{m}$ (Fujita and Wakimoto, 1981; Hjelmfelt, 1988). For low-rise buildings (for which eaves height will be below $z_m$), the eaves height wind-speed has the same significance as for ABL winds. For high-rise buildings (for which eaves height is above $z_m$), the eaves height wind-speed is not the maximum on the windward face; the peak maximum speed takes this role. It may be argued that the peak maximum speed is the better choice when comparing pressure fields on buildings of different heights subject to downbursts, or when comparing high-rise buildings subject to downbursts with those in ABL winds; conversely the eaves height wind-speed is arguably better for comparison of pressure fields on low-rise buildings exposed to downbursts and ABL winds. An alternative for downbursts is to use the downdraft velocity (herein referred to as $V_j$ due to its being the equivalent of the jet velocity in impinging jet simulations), though this is problematic for full-scale events as it is not directly measured and must be estimated. The normalising velocity used by each group of researchers is stated where their results are mentioned in Section 4.

Chay and Letchford (2002a) examined the differences between the centreline pressure coefficients on a cube (calculated using $p_{ref}=p_{atm}$, and the jet velocity for normalisation) at 0° yaw angle for downburst (steady impinging jet) and ABL winds, illustrated in Fig. 1 (where $C_{pe} \equiv C_p$ and $X$ is the radial distance from the centre of the downburst). Windward wall pressure coefficients are higher for downburst winds, and more uniform. For $X/D=0.75$ (relative distance from the downburst impact), suction is approximately 30% smaller on the roof at the leading eave compared to ABL flow. Chay and Letchford partly ascribe the differences over the roof to the difference in turbulence intensity, with the uniform, downburst and ABL flow cases having turbulence intensities of $<5\%$, 20% and 27%.

The advances made through this and similar research, encouraged reflection on how transient winds should be analysed. Downburst outflow is radial, with the radial velocity represented herein by $U$. Traditional analysis methods and parameters (e.g., turbulence intensity, spectral power density, etc.) assume a stationary time series which, by definition, is not the case for a transient event. In order to make use of these parameters, methods have been employed which split the time-series into at least two parts, one representing the underlying velocity trend, $U(t)$, and the other the turbulent fluctuations about this trend, $u'(t)$. The former may be approximated by using a running mean (e.g. Holmes et al., 2008) or the low-frequency levels of a discrete wavelet transform (e.g. Wang and Kareem, 2004; Wang et al., 2013) and removed from the time-series to leave only the fluctuations. Alternatively, a "detrended" time-series may be derived by splitting the time-series into sub-sections, each of which has an identifiable trend which may be removed (Orwig and Schroeder, 2007). The method used in the current research is similar to that of Wang and Kareem, and so this will now be discussed in more detail. In place of the standard definition of turbulence intensity for a stationary signal, $I_u$

$$I_u = \frac{\sigma_u}{U} \tag{3}$$

in which $\sigma_u$ is the standard deviation of $U$, Wang and Kareem proposed a windowed version

$$I_{u,T}(t) = E\left[\frac{\sigma_{u,T}}{U_T(t)}\right] \tag{4}$$

giving an instantaneous value of $I_{u,T}$ at time $t$. $I_{u,T}(t)$ is the expected value of the instantaneous turbulence intensity calculated using a time-varying mean, $U_T(t)$, over a window of width $T$. This gives a turbulence intensity time-series – if applied to a stationary signal, the standard definition of $I_u$ is simply the expected value of this time-series; i.e. it is $I_{u,T}$ with a single window spanning the entire time-series. Whether a running mean or wavelet approach is used to determine $U_T(t)$, there is an element of subjectivity in deciding the boundary between the turbulent and mean components, though Wang and Kareem did attempt to avoid this by comparing the probability density function (pdf) of the turbulent component to a Gaussian distribution.

Despite the large effort expended in simulating downburst-type events, there has been little explicit acknowledgement in the wind engineering literature of the variability that exists with such phenomena, and the corresponding implication that this can have on the near ground wind speeds. This may perhaps be attributed to the dearth of appropriate full-scale measurement with data captured at Andrews Air Force Base (AAFB) (Fujita, 1985), the Texas Rear Flank Downdraft (TRFD) (Gast and Schroeder, 2003; Orwig and Schroeder, 2007) and Tuas, Singapore (Choi, 2004) and by Lombardo (2011) being the exception. Interestingly, the Lombardo work clearly highlights such variability. McConville et al. (2009) illustrated the variability which can occur between different experimental runs of an impinging jet, transient wind simulator. Their work focused on generating an ensemble average which was then compared with the AAFB data, and this ensemble approach is maintained in the current research. While an averaging method such as this may seem inappropriate for the investigation of forces on structures, in which maximum aerodynamic forces may be deemed of greatest importance, it is shown later that, due to the velocity scaling, the force coefficients calculated from the ensemble approach are comparable to those from a single run "maximum". The ensemble approach then permits amalgamation of results, as will be explored in more detail later.

Despite the advances made to date in this field, there is still work required in order to understand not only the structure of transient winds but also their interaction with engineering structures and the corresponding implications of these interactions. The current paper will address these issues (at model scale) for two engineering structures, i.e., a typical portal-framed structure and a cube. However, before such interactions are examined, Section 2 will briefly outline the experimental facility used while Section 3 will examine the profiles of the generated wind velocities. Section 4 outlines the aerodynamic pressure and forces coefficients on both structures while appropriate conclusions are drawn in Section 5.

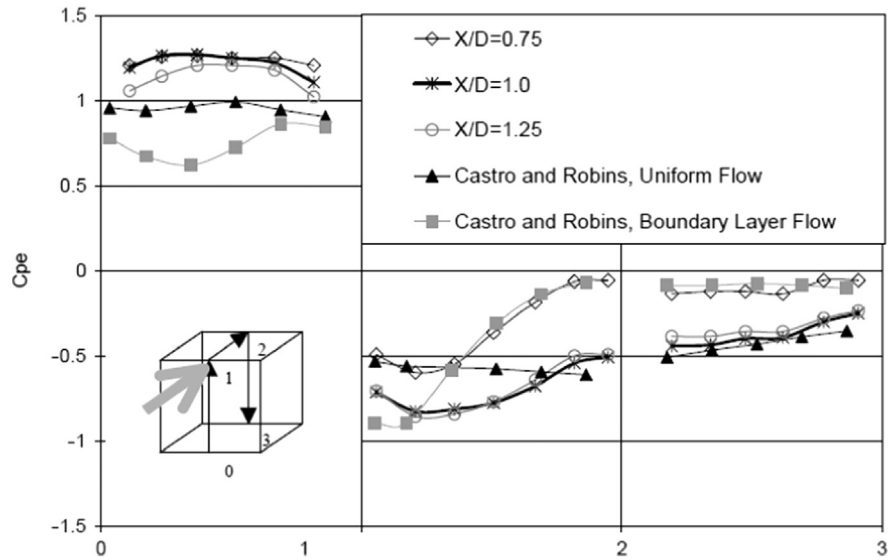


**Fig. 1.** Pressure coefficients in ABL and downburst winds (from Chay and Letchford (2002a); peak maximum downburst velocity at $X/D=1.0$).

## 2. Experimental facility

The (impinging jet) experimental facility used for the current work is outlined in detail in McConville et al. (2009) but is briefly described below. Nine axial flow fans, each of cross-sectional area 0.85 $m^2$, direct air into a settling chamber. The fans are located 4.5 m above the ground and direct air vertically downwards. A honeycomb grid is located directly below the fans in order to aid in the removal of swirl generated by the fans. Directly below the settling chamber is a transition section which accelerates the air and results in a circular jet of diameter ($D$) 1 m. Immediately below the transition section is an opening mechanism consisting of 8 flaps which are computer controlled and, in conjunction with direct control of the fans, generate the transient winds. The downflow impinges onto a raised horizontal ground plane, approximately 100 mm above the laboratory floor. This raised plane allows instrumentation to be fitted below the plane. The plane is made of smooth PVC sheeting. Surface roughness has been shown to affect the height of $z_{max}$ and formation of the secondary vortex (Mason et al., 2009b) but not the shape of the primary vortex (Vermeire et al., 2011). However, in the current arrangement, the distance from the point of impingement to the location of the maximum wind speed is relatively short indicating that surface roughness is not a governing factor in the current simulations. In addition, the data in Section 3 illustrates that the scaled height of $z_{max}$ in these simulations is comparable with that of full-scale events. A schematic of the facility is shown in Fig. 2. The velocity of the jet ($V_j$) immediately below the transition section attains a mean value of 13.7 $ms^{-1}$, with a corresponding turbulence intensity (standard deviation/mean) of 13%. The jet velocity has been shown to be uniform, with negligible variation over a radial distance ~0.45 m from the centre of the 0.5 m radius downdraft (McConville, 2008).

As discussed by Sterling et al. (2011), scaling such transient winds is not straightforward and is open to interpretation. This issue is compounded by the variation seen in the full-scale data, where downdraft diameter estimates range from 1 km to 3 km (Lin, 2010). Furthermore, "complete" full-scale data sets, with anemometer measurements at a range of lateral and vertical spacing to directly infer the downdraft diameter are not, to the authors' knowledge, available. Two data sets, from the AAFB and TRFD events, are combined here to permit an estimate of velocity and length scales, and from these a time scale is inferred. The static pressure field under and around a downburst consists of a series of concentric, alternating rings of high and low pressure around a high pressure

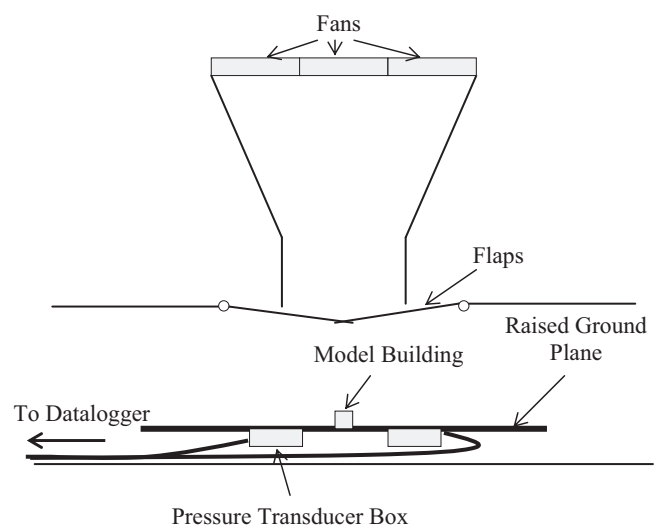


**Fig. 2.** A schematic of the transient wind experimental facility.

dome underneath the downdraft (Fujita, 1985). The pressure field recorded at the time of the downburst may therefore be used to estimate the diameter of the downdraft. The AAFB data is used here to determine scales and its downdraft diameter has been estimated as "<2000 m" (Lin, 2010) and 2000 m (Holmes and Oliver, 2000) using this pressure method. Inspection of the pressure field diagram provided by Fujita (1985), and noting that the marked low pressure ring is of greater diameter than the downdraft itself, leads the authors to an estimate that a value of $D=1600$ m is not unreasonable. Such a value yields a length scale based on this diameter of 1:1600. Determination of a velocity scale between the simulation and AAFB data is complicated by the heights at which the two sets of data were measured: the lowest height for these simulations corresponds to ~16 m full-scale (based on the 1:1600 length scale), while the AAFB data were measured 5 m above the ground. The TRFD data set, however, includes anemometer measurements from an array of towers, including measurements at 3 m, 4 m, 6 m, 10 m and 15 m, and 4 m, 6 m and 10 m on Towers 4 and 5 respectively (their designations; see Gast and Schroeder, 2003; Holmes et al., 2008). Analysis of the data at each height (not shown) indicates that the maximum velocities seen at 5 m and 15 m differ by only ~6%, a negligible amount in the context of this scaling exercise. Based on

this, and assuming that the same profile is applicable to the AAFB event, the 5 m data may be taken as an approximation to the wind speeds at 15 m. The ratio of the maximum radial velocity, $U_{max}$, to the downdraft velocity in the physical simulations for the current work was $U_{max}/V_j \approx 1.7$ (Fig. 3, plotted with a non-dimensional timescale, $t^*$, where $t^* = t(D/V_j)$ and t is the actual time). In the case of the full-scale event the wind speed is non-zero leading up to the downburst, with a mean value of $\sim 6\ \mathrm{ms}^{-1}$. This value has been subtracted from the AAFB time-series giving a maximum full-scale velocity (excluding the base wind) of $\sim 61\ \mathrm{ms}^{-1}$. Assuming that the $U_{max}/V_j \approx 1.7$ ratio is applicable for the full-scale event, a downdraft velocity of ca. $36\ \mathrm{ms}^{-1}$ is calculated. This gives a velocity scale of approximately 1:2.6. Combining these two ratios gives a time scale of approximately 1:600, which appears reasonable when the initial gusts are compared (Fig. 3). The rapid increase in velocity associated with the passing of a primary (ring) vortex is evident in Fig. 3 at time $t^* = 16$, which will be discussed further in Section 3.

Velocities were measured using Cobra probes, manufactured by Turbulent Flow Instrumentation (TFI). These probes have a response cut-off frequency of 2 kHz, above which the signal is attenuated. The recorded velocity time-series were smoothed using a 50-point moving average, which corresponded to approximately 3 s at full-scale. Velocity measurements were made at a range of radial distances, $x$, from the centre of the downdraft, with $x/D = 1.0$, 1.25, 1.5, 1.75, 2.0 and 2.5, at 10 mm (16 m full-scale) vertical increments spanning 0.01–0.25 m (16–400 m full-scale) from the ground plane. The maximum velocity was seen to occur at $x/D = 1.5$, at a height of $z/D = 0.02$ (this is illustrated and discussed further in Section 3).

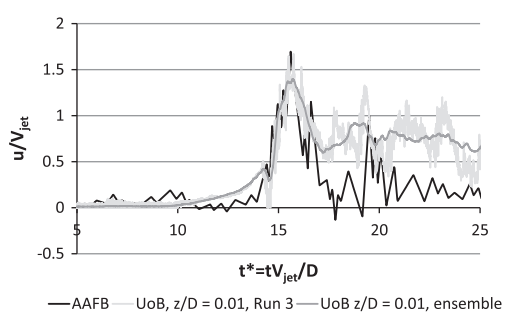


**Fig. 3.** Non-dimensionalised radial velocity time-series for the UoB simulations and the AAFB full-scale event.

Two model buildings were used for this research, each 3-D printed with built-in pressure tappings. Fig. 4 and Table 1 illustrate the two model structures and corresponding dimensions respectively used in the experiments. The 60 mm cube allows comparison with the work of Chay and Letchford (2002a), based on the same ratio of cube dimensions to jet diameter ($D$). The position of the models relative to the impinging jet are shown in Fig. 5, which also indicates the co-ordinate system adopted in the current work: $x$ represents the distance from the centre of the impingement in the mean flow direction; $y$ is the lateral distance measured perpendicular to $x$; $z$ is the vertical distance which is perpendicular to the $x$–$y$ plane. The velocity field is represent by $u(t)$, $v(t)$ and $w(t)$ which correspond to the velocities at time $t$ in the $x$, $y$ and $z$ directions respectively. Capitals, e.g. $U$, are used to represent running mean values. Pressures were measured over the surface of the model buildings and at five locations on the ground plane, along the radial line passing through the centre of the building (Fig. 5). The pressure was measured at a rate of 500 Hz using a bespoke, 64-channel digital pressure measurement system (DPMS), designed and manufactured by Solutions for Research Ltd. The DPMS is based around Sensor-Technics HCLA12 × 5DB pressure transducers, with an operating differential pressure range of 1250 Pa and a maximum uncertainty of ±0.25% of the Full Scale Span (1250 Pa), i.e. ±3 Pa (Sensor-Technics, 2014). The building tappings were connected to the DPMS with 1.35 mm (inside diameter) tubes of length 0.6 m, with 1 m long tubes used for the ground plane tappings. This tube length is relatively long, but was the minimum required to span the longest connection distance, and it was considered preferable to use equal length tubes for all the building connexions. Possible attenuation of the pressure signals was investigated by taking pressure measurements using a short piece of metal tube held in a retort stand, located just upstream of the building position, as a simple Preston tube. This was connected to a single channel of the DPMS using a 0.05 m tube and five runs of the simulator recorded. This process

**Table 1**
**Model building dimensions.**

| Model | Height (mm) | Width (mm) | Length (mm) |
|---|---|---|---|
| Portal | 42 (eaves) 53 (peak) | 130 | 240 |
| Cube | 60 | 60 | 60 |

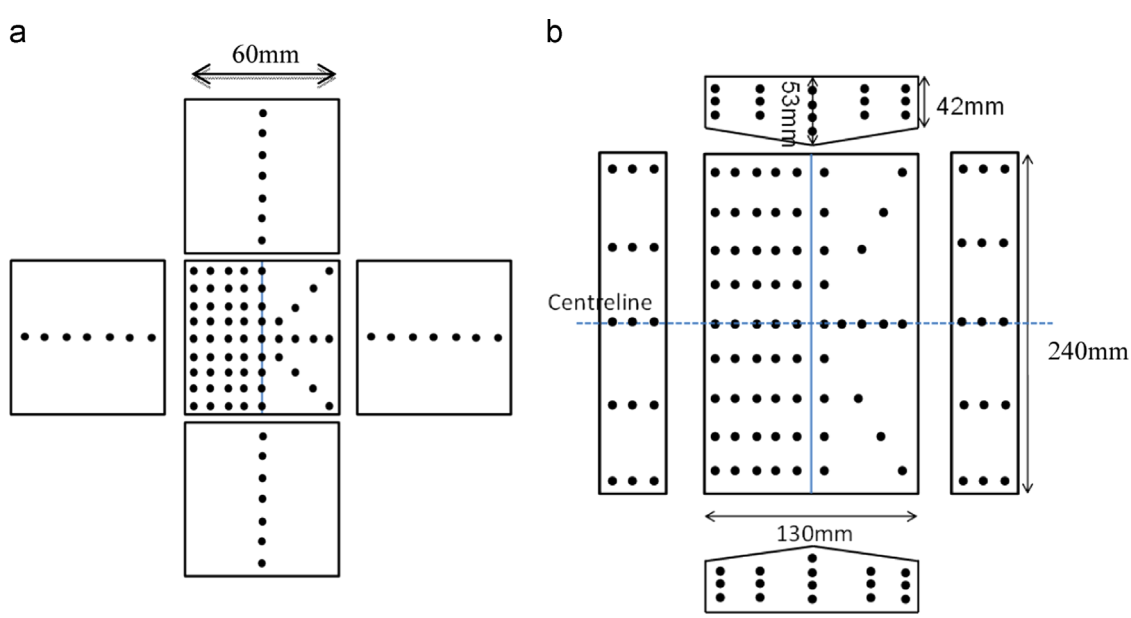


**Fig. 4.** The model building pressure tappings (not to scale). (a) 60 mm cube and (b) portal frame.

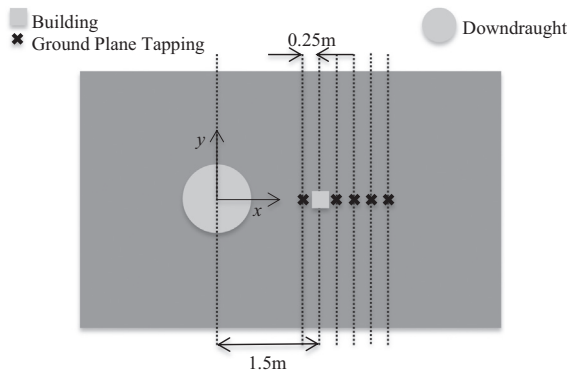


**Fig. 5.** Plan view schematic of the building and ground plane pressure tapping locations, with *x*- and *y*- axis definition. The *z*-axis is out of the page.

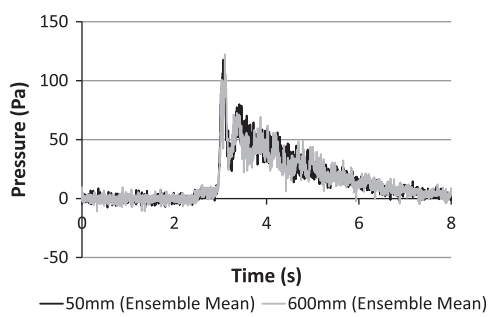


**Fig. 6.** Pressure time-series with 50 mm and 600 mm tubes.

was repeated with a 0.6 m tube (only four run included in the 0.6 m tube analysis as one run was found to have mis-recorded). The maximum values of the ensemble mean time-series were 117.9 Pa and 122.4 Pa respectively, a difference of ~4% (Fig. 6) and one which falls inside the transducer uncertainty. Further, applying a *t*-test analysis to the maxima of the individual runs gives an 80% chance of equivalency of the means. As this study is examining only the maximum loading on the building models, frequency response due to tube resonance is not particularly relevant or indeed significant to the current work. As with the velocity time-series, the data was smoothed using a moving average equivalent to a gust of approximately 3 s duration at full-scale, in this case a 3-point average.

For both the pressure and velocity measurements, a multiple-run, ensemble-mean approach was used. Vertical velocity profiles were constructed by positioning the Cobra probe at a height, *z*, performing ten experimental runs (following McConville et al., 2009) and then moving the probe and repeating for the next *z*. Taking the ensemble allows features which are consistently seen across the ten runs to be elucidated – inspection of data from a single run does not discriminate between turbulence effects specific to that run and more general features. Pressure data was gathered using a similar ensemble approach, with the signal from the first ground plane tapping used to synchronise all 64 channels of the DPMS. The ensemble approach was also of benefit here – with more than 64 tappings on the building, roof and wall pressures were measured separately and the two sets of ensemble data combined to give the pressure distribution over the entire model.

## 3. Transient wind simulation

The velocity field was mapped at a number of radial distances from the centre of the downdraft, as discussed in Section 2. Analysis of the flow field shows that the peak maximum radial velocity, $U_{max}$, was found to lie at $x/D=1.5$ and only this radial position is considered for the pressure measurements. As illustrated in Fig. 7, the vertical distribution of *U* velocity (non-dimensionalised by the maximum velocity, $U_{max}$, and plotted against a vertical position ordinate non-dimensionalised by $z_m$) lies within the envelope of the full-scale data collated by Hjelmfelt (1988), although it is noted that the "nose" of the profile is widened (more constant with height). Error bars have been included in this figure for the current data (labelled "UoB"), based on the manufacturers stated accuracy of the Cobra probes of $\pm 0.5\ \mathrm{ms}^{-1}$ (a value independently verified by Mallipudi et al. (2004)). Within this uncertainty, all points fall within the envelope of full-scale events. Within the uncertainty indicated, $U_{max}$ occurred over a 20 mm high region centred at a height above the ground plane of $z=z_m=0.02$ m (i.e. $z_m=20\ \mathrm{mm} \pm 10\ \mathrm{mm}$).

The vertical centre of the maximum velocity region lies at $z_m/D \sim 0.02$, corresponding to a full-scale height of ~30 m, assuming a 1:1600 length scale. This lies within (though at the lower edge) of the range of 30–100 m given for full-scale data (Fujita and Wakimoto, 1981; Hjelmfelt, 1988).

As a downburst is a highly non-stationary event, modelling the unsteady nature of the flow field is important. Comparison with full-scale data is difficult due to the transient nature of full-scale events and the need to estimate scaling parameters. As presented in Section 2, length, velocity and time scales of 1:1600, 1:2.6 and 1:600 are estimated for this simulation based on the AAFB full-scale event. Applying these values to non-dimensionalise the full-scale data shows good agreement, over the region of interest, between the AAFB data and the simulations (Fig. 3), with similar acceleration rates at the leading edge of the downburst. In addition, a continuous wavelet transform, using a Morlet wavelet, has been applied to both the simulation and AAFB data and shows a reasonable match (Jesson et al., 2013) in both dimensionless time and frequency.

The dimensionless maximum velocity seen in the ensemble-mean time-series is slightly lower than the full-scale equivalent data, though this may be explained by the averaging processes involved in calculating the ensemble mean, and the subsequent smoothing. The turbulence intensity (TI) was calculated for each of the ten runs at $z/D=0.02$. As noted earlier, for a non-stationary signal TI is not formally defined, and several methods have been suggested to address this. For this study, a similar approach to the discrete wavelet transform (DWT) method of Wang and Kareem (2004) was applied, taken to the limit of $T=1/(\textit{sampling rate})$, i.e. the window is a single sample. A Daubechies-10 wavelet was used for the DWT, with 15 resulting frequency levels (indexed as −1 to 13, low to high frequency). The residual component, $u'(t)$, corresponding to the

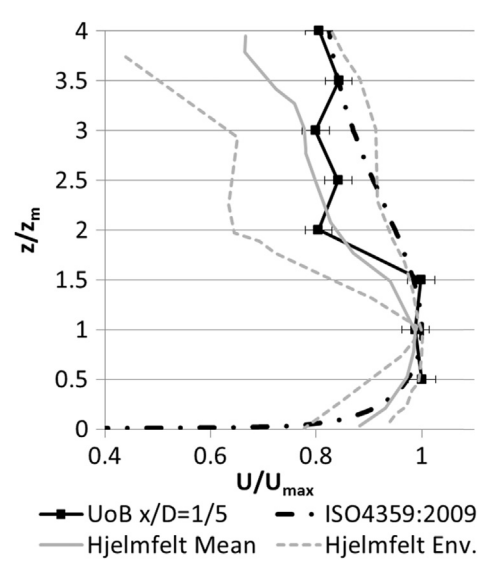


**Fig. 7.** Vertical velocity profiles – UoB, full-scale (mean and upper and lower envelopes from Hjelmfelt (1988)) and the ISO4359 thunderstorm profile.

turbulence, was calculated as the sum of levels $n$–13, where level $n$ is the boundary level between the non-turbulent and turbulent frequencies. Levels of lower frequency than level $n$ are taken to be long-term trends contributing to the moving average; levels of higher frequency are taken to be turbulent fluctuations. Clearly, determining the correct boundary level, $n$, is key to the TI calculation.

The mean of the turbulent component, $u'(t)$, should be zero, and this criterion was used to identify the correct value of $n$. For each of the ten runs at $z/D=0.02$, $u'(t)$ was calculated for each possible boundary level, $n=1$ up to $n=13$. The mean value of $u'(t)$ during the downburst was calculated in each case. The lowest $n$ (i.e. lowest boundary frequency) for which this mean was approximately zero (less than 0.01% of the maximum velocity) was determined. Over the runs examined, it was found that $n=8$ should be used for the calculation of $u'(t)$; equivalently, the time-varying mean, $U(t)$, is the sum of levels $-1$ to 7, with the latter corresponding to a non-dimensional frequency of $\sim 6$.

Mean and maximum TI values have been calculated for each run, with a representative run shown in Fig. 8. Holmes et al. (2008) calculated the mean TI during the period when the velocity exceeded 25 $\mathrm{ms}^{-1}$, equivalent to $U(t) > 0.7U_m$, and this approach has been used here to enable a comparison; the maximum is simply the maximum of all values. Over the 10 experimental runs examined, these mean and maximum TI values range from 3% to 6% and 15% to 26% respectively (Table 2). Higher values correspond to periods of low velocity such as the "dip" seen at $t^* \sim 15$ in Fig. 3, and following the maximum velocity. Holmes et al. (2008) found a higher value ($\sim$11%) for the TRFD data during the period of increased velocity, though this has been shown to be due to the calculation method – if the current DWT method, with a dimensionless frequency of $\sim 6$ used as the upper limit of levels contributing to $U(t)$, is applied to the TRFD data then a mean TI value of 6% is found, which lies within the range of values seen for the UoB data. Conversely, if Holmes' running-mean approach is applied to the UoB data then a TI of $\sim$10% is found (Table 2), which is close to the TRFD value. This highlights the problems with TI calculation for a non-stationary data signal, and the need for a standard method to be agreed upon and adopted.

In order to understand the structure of the primary vortex in detail, the radial and vertical velocity time-series have been plotted together for two heights at $x/D=1.5$, $z/D=0.02$ and $x/D=1.5$, $z/D=0.20$ (Fig. 9). It is clear, particularly in the $z/D=0.20$ case, that the periods of high radial velocity are consistent with the passage of a vortex, with upward flow preceding $U_m$ and downward flow following it. Close to the ground, $z/D=0.02$, vertical flow is inhibited by the ground plane; conversely, distant from the ground plane, at $z/D=0.2$, a significant vertical component to the velocity field is evident.

The passing of the vortex may also be elucidated using phase-plots, in which instantaneous values of horizontal and vertical velocities at a given location are plotted for all $t$. In the case of two random signals the phase-plot will show a random pattern; in the case of correlated signals the phase-plot will exhibit order, though temporal scale is lost. The coherence of the radial and vertical velocities at four $x$ positions may be seen in Fig. 10. Whereas the peak maximum $u(t)$ is seen at $x/D=1.5$, the maximum $w(t)$ occurs at $x/D=2.0$, which matches the findings of Hjelmfelt (1988) who, from his examination of the JAWS full-scale data, determined that the vortex was not fully formed at the time of the maximum velocity. The results for $x/D=1.0$ indicate an increase in the diameter of the impinging jet with distance from the nozzle as all vertical velocities are still downwards.

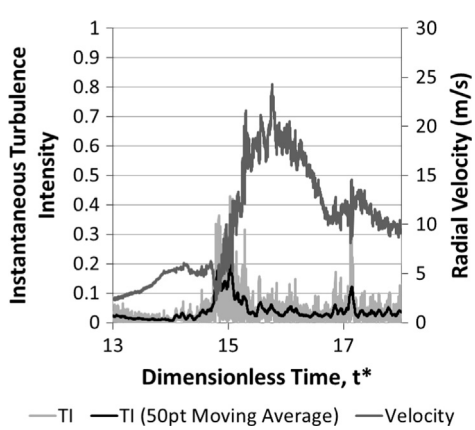


**Fig. 8.** Turbulence intensity during a single run at $z/D=0.02$.

## 4. Aerodynamic pressure and force coefficients

Wind loading, in the form of radial (drag, $x$), and lateral ($y$) force coefficients and vertical ($z$) uplift coefficients, are discussed in this section. Following this, the instantaneous pressure coefficient distributions measured over the surfaces of the two model buildings (the 60 mm cube and portal frame) at the time of the maximum magnitude of vertical uplift (roof suction) will be presented, with comparisons made with the work outlined in Section 1 where applicable. Animations showing the variation of the instantaneous $C_p$ distribution during the simulated downburst event are available for viewing online at www.birmingham.ac.uk/transient-winds.

Due to the peak maximum velocity occurring at $z_m = \sim 0.02$ m, the maximum velocity on the windward edge is below the eaves height of both models and so the peak maximum velocity (19.4 $\mathrm{ms}^{-1}$) has been used as the normalising velocity in Eq. (1). This approach was also used by Butler et al. (2010), while Chay and Letchford (2002a), Sengupta et al. (2008), Mason et al. (2009a) and Zhang et al. (2013) all used $V_j$ as the normalising velocity. It is a simple matter to scale the data from the latter studies using their reported peak maximum and jet velocities – the rescaled values are used in this discussion. With the exception of Mason, these studies have used steady impinging jets (albeit translating in some cases) and so have not simulated the primary, ring vortex which occurs during a downburst. Pressure coefficients have been calculated using $p_{atm}$ (measured at a location in the laboratory away from the model location and transient flow field) as the reference pressure – unless otherwise stated the values presented from previous work have been calculated in the same manner.

### 4.1. Wind loading on cubic and portal framed buildings

Force coefficients have been calculated using Eq. (2) and the ensemble mean pressure measurements, with an estimated uncertainty of $\pm$10%, based on the uncertainties of the pressure and velocity measurements. The radial drag on the cube has a value of approximately unity for both 0° and 45° yaw (Fig. 11). Peak lateral force is of slightly greater magnitude (0.25 versus 0.18) for 45° yaw, and in both cases the lateral drag alternates sign. This change of sign may be evidence that vortex shedding is taking place even though the flow is transient. At the Reynolds number ($\sim 8 \times 10^4$, based on the building length in the radial direction and maximum radial velocity) seen in the simulations, the Strouhal number for a cubic building is $\sim$0.13 (Sohankar, 2006). This gives a theoretical dimensionless time between vortices of 0.32 – this matches closely with the value of $\sim$0.3 between the high magnitude positive and negative lateral forces seen in Fig. 11. The magnitude of the uplift, $\sim$0.57 and 0.54 for 0° and 45° yaw respectively, is the same within the uncertainty level. The magnitude of the lateral force increases at a lower rate than that of the radial drag, with a sharp peak at the maximum rather than the plateau seen for the latter.

**Table 2**
**Mean (during the period of increased *U*) and maximum TI values calculated for the UoB data using the DWT and Holmes' methods.**

| | Run 1 | Run 2 | Run 3 | Run 4 | Run 5 | Run 6 | Run 7 | Run 8 | Run 9 | Run 10 | Mean |
|---|---|---|---|---|---|---|---|---|---|---|---|
| UoB DWT method | | | | | | | | | | | |
| Mean (%) | 3 | 4 | 3 | 5 | 3 | 3 | 4 | 4 | 3 | 6 | 4 |
| Max. (%) | 23 | 21 | 26 | 15 | 24 | 17 | 21 | 23 | 15 | 23 | 21 |
| Holmes' method | | | | | | | | | | | |
| Mean (%) | 9 | 10 | 11 | 11 | 10 | 11 | 13 | 9 | 10 | 10 | 10 |
| Max. (%) | 13 | 16 | 18 | 14 | 27 | 15 | 29 | 19 | 22 | 17 | 19 |

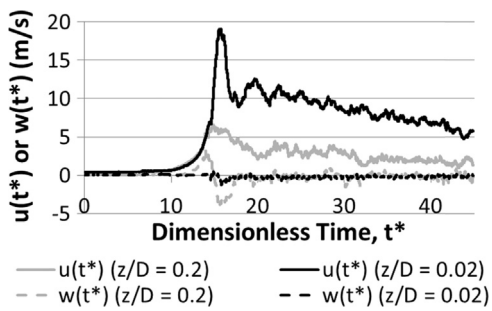


**Fig. 9.** Radial and vertical velocity time-series at $x/D=1.5$, $z/D=0.02$ and $z/D=0.2$.

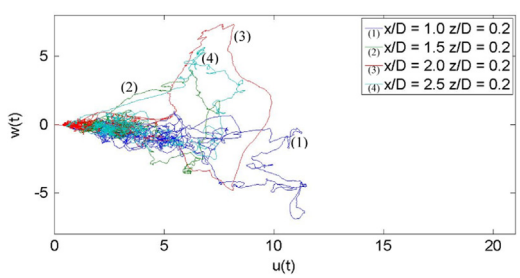


**Fig. 10.** $u(t)-w(t)$ phase-plot at $z/D=0.2$ and $x/D=1.0$, 1.5, 2.0 and 2.5.

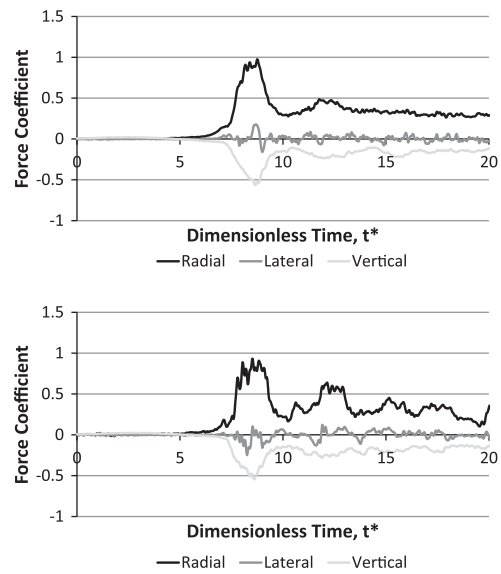


**Fig. 11.** Force coefficients on the cube with 0° (top) and 45° (bottom) yaw. For consistency with the sign of $C_p$, negative vertical force is an uplift.

With the portal-framed building, radial drag is lower than that seen for the cube, having values of ~0.5, 0.6 and 0.5 for the 0°, 45° and 90° yaw angles respectively (Fig. 12). This is attributed to the lower building height. The 0° value is greater than that measured by Zhang et al. (2013), though their 90° value was ~80% greater than that measured for 0°, counter to the results shown here. Lateral drag is negligible ($\leq 0.1$) but there is evidence of alternating positive and negative pressures as for the cube, particularly for 0° yaw when the longest sides of the building face the lateral direction. Roof uplift magnitude were ~0.4, 0.4 and 0.3 for the three yaw angles respectively; the former is equal to that seen by Zhang el al. though they found equal values for 90° yaw. The variation seen in the current work may therefore be due to the rectangular (as opposed to Zhang et al.'s square) base shape, with different radial (along-wind) lengths for the two yaw angles. Further studies are required to clarify these differences.

### 4.2. Pressure fields on cubic buildings

To aid comparison with previous work, centreline pressure coefficients are shown in Fig. 13 for the current and earlier studies examining cubes at 0° yaw (i.e. the cube has one face perpendicular to the radial outflow). The values shown for the UoB work correspond to the instant of the maximum magnitude of the lift coefficient. The characteristic parameters of these studies are given in Table 3, from which it can be seen that, based on the ratio of jet diameter to cube size, Chay and Letchford (2002a) and Mason et al. (2009a) have approximately equal scales to the current work.

On the windward face, the current study has a maximum $C_p \approx 0.6$. This is approximately 40% lower than the value seen in the steady impinging jet study of Chay and Letchford (2002a), and approximately 30% lower than that seen by Mason et al. (2009a). In the latter case, Mason et al. note that their opening mechanism was probably causing acceleration of their jet, and causing underestimation of their $V_j$ value. Differences between the Chay and Letchford's results and those of and the current study may be due to the very different nature of Chay and Letchford's steady flow and the ring vortex structure seen in the current study. In the current study, the maximum $C_p$ is found at the midpoint of the windward face, with a reduction closer to the ground before a small increase at the base of the cube. This pattern is similar to that seen by Richards et al. (2001) for ABL flow, although magnitudes are lower in the current study.

Richards et al., Chay and Letchford and Mason et al. all found $C_p$ to decrease with distance from the windward edge of the roof, with maximum suctions approximately one quarter of the roof length from the leading edge. The decrease in suction is greater in Richards et al.'s ABL case, and a lower magnitude $C_p$ is seen on the rear half of the roof than the front. The current study shows a more symmetrical pattern, with the maximum suction occurring approximately in the centre of the roof and values at the windward and leeward edges approximately equal. This suggests that the localised separation followed by downstream reattachment seen in steady flows is not present in the transient, ring vortex-driven pressure field of the downburst. On the windward half of the roof, suctions are greater in the steady state cases than in the pulsed jet studies, but the pressure quickly starts to recover and is greater than the pulsed jet values by

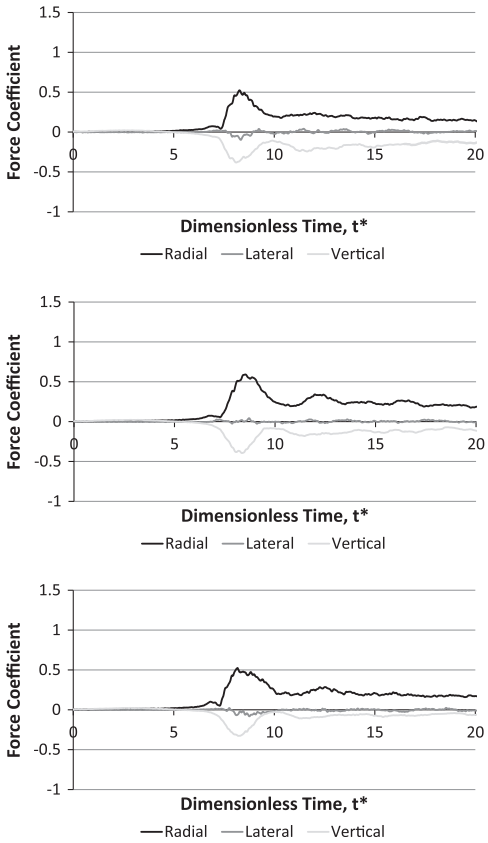


**Fig. 12.** Drag coefficients on the portal building with 0° (top), 45° (middle) and 90° (bottom) yaw. Refer to the caption for Fig. 11 for more information.

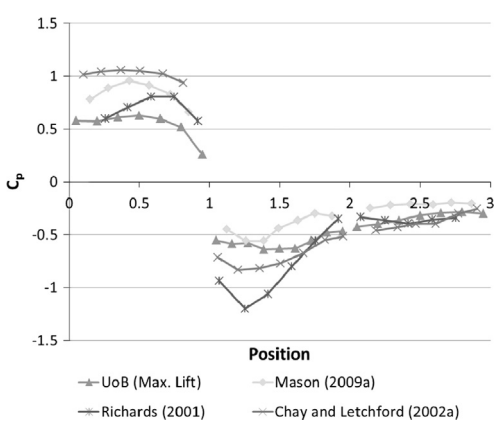


**Fig. 13.** Centreline pressure coefficients over a cube at 0° yaw during simulated thunderstorm downbursts and full-scale ABL flow. Position is normalised by the cube size.

**Table 3**
Summary of the dimensions of experiments to measure pressures on cubes wth 0° yaw angle (N/D – No Data).

| Study | Flow type | Jet diameter (m) | Cube size | $U_{max}/V_j$ | TI (%) |
|---|---|---|---|---|---|
| Current | Pulsed impinging jet | 1.00 | 60 mm | 1.6 | 5 |
| Chay and Letchford (2002a) | Steady impinging jet | 0.51 | 30 mm | 1.0 | 20 |
| Sengupta et al. (2008) | Steady impinging jet | 0.20 | 25 mm | 1.0 | N/D |
| Mason et al. (2009a) | Pulsed impinging jet | 0.51 | 30 mm | 1.6 | N/D |
| Richards et al. (2001) | Full scale ABL | N/A | 6 m | N/A | 20 |

the leeward roof edge. Such differences in flow separation and reattachment are often attributed to differences in TI, and indeed the data of Chay and Letchford and Richards et al. (with similar TIs – Table 3) show more similarity than that of the pulsed jet studies. Significant differences in magnitude are, however, still apparent between the data sets of Chay and Letchford (2002a) and Richards et al. (2001), indicating that other factors, such as the vertical velocity profile, may be affecting the pressure field. The reduced windward edge flow separation seen in the pulsed jet data of both Mason and the UoB may be due to the region of high TI which precedes the maximum radial velocity (Fig. 8).

Moving over the leeward eave, $C_p$ is reasonably continuous and $C_p$ is more uniform over the leeward face than the windward face. The range of absolute, leeward face $C_p$ values seen across all these studies is much smaller, though (for example) the values seen by Richards et al. are approximately twice those seen by Mason et al.

The full pressure field over the cube (corresponding to the time of maximum lift) is shown in Fig. 14. At 0° yaw angle there is large negative pressure on the side faces (2 and 4), with $C_p \approx -0.85$ and $C_p \approx -0.60$ respectively. This imbalance between the negative pressures on the two sides may be due to vortex formation and shedding occurring alternately on each side. Fig. 14 captures the pressure coefficients at an instant in time, at which point vortex formation will be at different stages on the two faces; in contrast, Fig. 11 shows the temporal variation in lateral force and shows its alternating direction. The negative pressure on face 2 has its minimum in the bottom third of the face, possibly due to the higher radial velocities in this region. Examining the roof as a whole, negative pressures are larger on the right-hand side of the roof, which may be due to either a slight misalignment of the model or asymmetry of the outflow.

At 45° yaw angle (Fig. 14b), positive pressures occur on the two windward faces (1 and 2), though the magnitude is much reduced when compared to the windward face for 0° yaw ($C_p \approx 0.3$ rather than $C_p \approx 0.6$), as would be expected. At the top of the leeward faces (3 and 4), $C_p \approx -0.6$ and $C_p \approx -0.3$ respectively, and this difference is matched in the values seen on the closest roof tappings. For both faces 3 and 4, $C_p$ tends towards $-0.4$ at the bottom of the face, i.e. it increases in magnitude with height over face 3 but decreases over face 4. This implies that the pressure field over the roof affects the negative pressure on the upper part of these faces. The negative pressure at the windward eaves increases in magnitude, with maximum suctions of $C_p \approx -1.0$ as opposed to $-0.6$ for the 0° yaw case (Fig. 14 and, more clearly, Fig. 15). This may be due to the formation of high intensity vortices at the leading edge (akin to delta wing vortices in ABL flow), with the suction reaching a maximum approximately one quarter of the edge length downwind of the corner, (similar results for ABL flow have been seen by, for example, Mehta et al. (1992)). Beyond this point, the delta vortex increases in diameter and its axis moves away from the roof edge, leading to the reduction in suction at the edge.

Despite this high leading edge suction seen at the windward eave for 45° yaw, the uplift coefficients are the same for both yaw angles (see Section 5). This illustrates an issue with using drag and uplift coefficients to represent forces over a large area – resolution is lost. Fig. 14b shows higher suction on the right-hand side of the leading edge than the left, again thought to be caused by either a slight misalignment of the model, or asymmetry of the outflow, though the suction is more uniform (with a greater minimum magnitude) over the left-hand side of the roof than the right.

### 4.3. Pressure fields on portal buildings

When the yaw angle corresponds to 0°, the maximum positive pressure coefficient is ~0.56 and occurs in the centre of the windward face of the portal building (Fig. 16a). On the two windward corners of the leading edge, local minima of $C_p = -0.5$ and $-0.6$

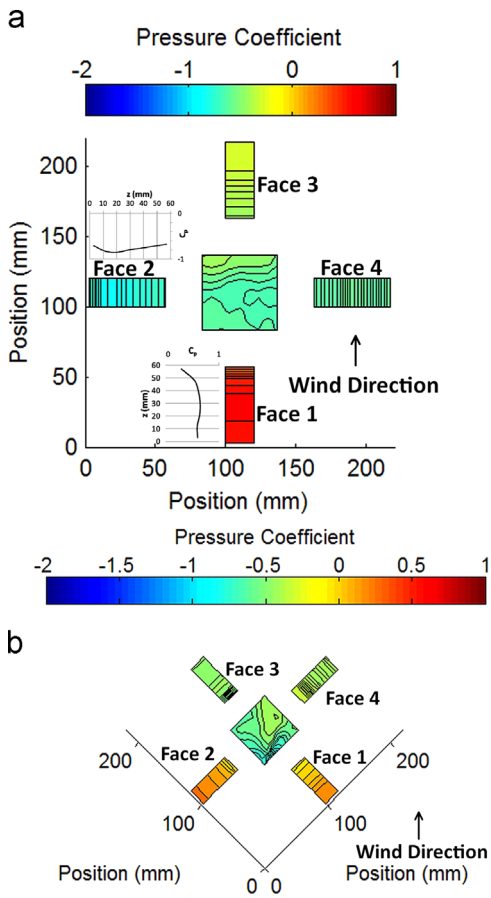


**Fig. 14.** Pressure coefficients at the time of maximum lift over the 60 mm cube with 0° (a) and 45° (b) degree yaw angles. Values have been interpolated for the untapped roof areas (see Fig. 4).

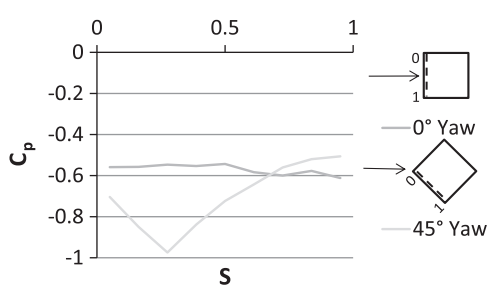


**Fig. 15.** Pressure coefficients along the windward roof edge of the 60 mm cube at 0° and 45° yaw. *S* is the normalised position along the edge, as indicated in the inset figures.

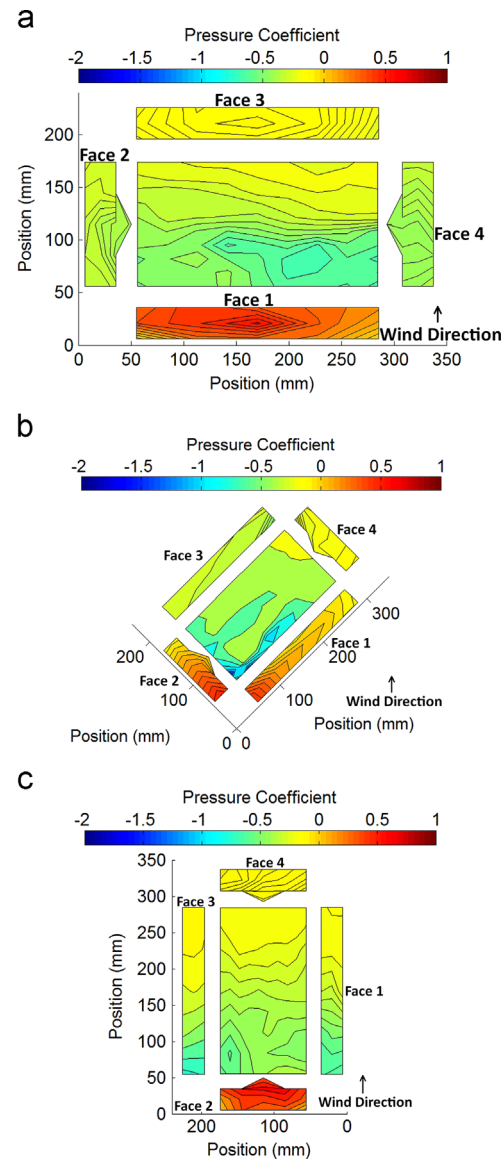


**Fig. 16.** Pressure coefficients at the time of maximum lift over the portal building with 0° (a), 45° (b) and 90° (c) yaw angles. Note that the plotting of these figures has caused distortion of the building shape – see Fig. 4. Values have been interpolated for the untapped roof areas (see Fig. 4).

were obtained. It should be noted that the animated distribution (see www.birmingham.ac.uk/transient-winds) indicates that the asymmetry seen in Fig. 16a is exaggerated, i.e., for the majority of the time the flow is approximately symmetrical. $C_p$ reduces towards the peak of the roof and over its back edge, with $C_p \approx -0.2$ at the leeward edge. The majority of the leeward face has $C_p \approx -0.1$, with $C_p$ increasing to as high as $-0.2$ towards the side edges. Suction is seen along the side faces, with $C_p$ ranging from $C_p \approx -0.3$ to $-0.4$ on face 2 and $C_p \approx -0.3$ to $-0.45$ on face 4. The higher magnitudes are seen in the windward third of the face and, in the case of face 2, towards the top of the face. The right-hand face has greater suction, again possibly due to asymmetry of the outflow. In their steady impinging jet simulations, Zhang et al. (2013) used two buildings as specified in Table 4. The proportions of these buildings differ from the building used in the current work, and only the 16° roof angle building is discussed here. In order to enable a comparison with the current work, the pressure coefficient data of Zhang et al. (2013) has been scaled by 1/1.44 (taking their $U_m/V_j \approx 1.2$). At $x/D=1.0$, their position of maximum radial velocity, Zhang et al. found higher maxima ($C_p \approx -0.7$) in the suction magnitudes, but a greater reduction in magnitude in the direction of flow due to reattachment. Roof pressure coefficients decreased from $-0.7$ at the windward eave to $\sim -0.35$ at the ridge, with an increase to $\sim -0.4$ behind the ridge and decrease to $\sim -0.1$ at the leeward eave. The ridge line increase in suction was not seen in the current study for 0° yaw. Similarly, suctions on the side faces reduced in magnitude at a greater rate than in the current study, falling from $-0.4$ at the windward end of the side face to almost zero at the leeward end.

With a 45° yaw angle, a maximum suction of $C_p \approx -1.4$ is seen at the leading roof edges (Fig. 16b and Fig. 17). Suction remains high ($\sim -0.7$) along the leading edges of the roof and, unlike the 0° yaw case, a region of increased suction ($\sim -0.6$) is seen along the back of the ridge line in the windward half of the roof. This ridge value is approximately equal to the value seen by Zhang et al.; the leading

**Table 4**
Portal building experiment specifications.

| Study | Flow type | Jet diameter (m) | Portal building size (mm) | Roof angle (°) |
|---|---|---|---|---|
| Current | Pulsed impinging jet | 1.00 | 42 × 130 × 240 | 10 |
| Zhang et al. (2013) | Steady impinging jet | 0.61 | 31 × 65 × 65<br>25 × 65 × 65 | 16<br>35 |

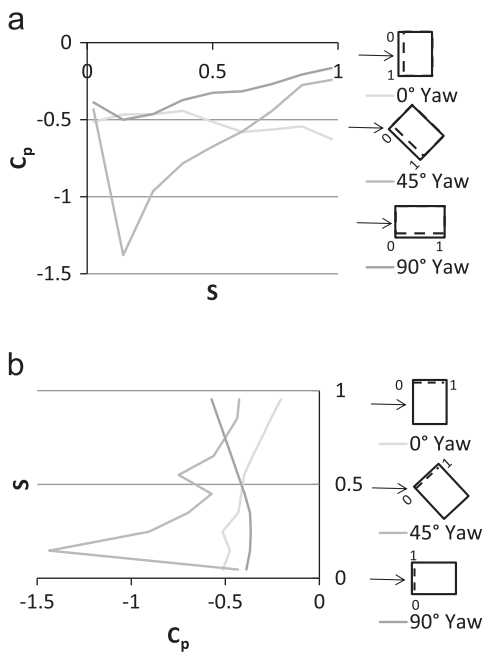


**Fig. 17.** Pressure coefficients along the portal framed building roof edges adjoining face1 (a) and 2 (b). *S* is the normalised position along the edge, as indicated in the inset figures.

corner suction is over double that seen by Zhang et al. The windward faces have a positive pressure at the leading edge (~0.4 and ~0.5 for faces 1 and 2 respectively), with suction at the trailing edge of $C_p \approx -0.1$ for both. The leeward faces (3 and 4) show the same pattern of increasing suction, though with suction the full length (−0.25 to −0.35 on face 3, −0.1 to −0.3 on face 4). Zhang et al. found similar magnitudes, but that the suction reduced along the wall in the direction of flow.

For the case of a 90° yaw angle (Fig. 16c), the roof centreline is coincident with the ridge, with the maximum ridge suction (~−0.45) occurring just downstream of the leading edge. From the radial midpoint of the roof, suction is approximately uniform laterally. In the windward half of the roof the field is more complex, with regions of high suction which spread towards the eaves. A localised increase in suction on the left-hand (looking with the wind) windward corner appears relative to the right-hand corner suction. However, this may simply be due to interpolation along the diagonal line of tappings which instrument this area (see Fig. 4), as no such increase is evident at the (better tapped) right-hand corner. $C_p$ reduces in magnitude along the length of the roof, with values of ~−0.2 at the leeward end. Similar suction values are seen along the side walls, with magnitudes equalling those on the roof at the same point. Suction at the windward end of the side faces (1 and 4) is stronger (~−0.6 and ~0.7 respectively) than that measured by Zhang et al. (~−0.55). Windward face pressure coefficients reach their maximum in the centre, near the roofline, with a value of ~0.6. In the bottom corners $C_p$ is <0.1, while in the middle of the face it is ~0.4. The leeward face exhibits suction with values from −0.08 to −0.11, with the higher values on the right-hand side; once again the reader is directed to the animated figures available online for a better insight into asymmetry of the pressure field.

## 5. Conclusions

For the first time, the pressure distribution over a cube and portal framed structure have been examined at model scale in a transient wind simulator generating the primary, ring vortex of a thunderstorm downburst. This novel research has highlighted the difficulties in scaling and thus comparing results undertaken in other physical experiments which have examined the aerodynamic forces on structures in steady impinging jets. The main findings of the current work are as follows:

- The current simulator is capable of creating the field velocities fields which are similar to those observed in nature.
- The mean turbulence intensity of the radial velocity varies between 3% and 10% depending on which method is used to calculate it.
- Phase-plots of the $u(t)$ and $w(t)$ components of velocity clearly illustrate the development of the primary vortex in the flow with respect to distance and height from the centre of the impingement.
- The aerodynamic force data for the cube show that the radial component of the drag illustrates similar trends between the 0° and 45° yaw, albeit with a greater degree of fluctuation for the 45° yaw. The 0° yaw represented the worst case in terms of overall lift force and strong evidence of vortex shedding was present in the lateral force coefficient for both cases.
- The aerodynamic force data for the portal frame building shows that the lateral component of force coefficient was close to zero throughout the entire time period for all yaw angles. Differences were observed in the uplift coefficients between yaw angles although these differences were within the uncertainty limits of the experiments. The radial drag is in general lower for the portal framed building than the cube.
- The pressure field corresponding to the time of maximum lift on the cube highlights a reasonably uniform distribution over the roof when the yaw angle is 0° in sharp comparison to the 45° yaw angle case. In the latter there is evidence of sharp gradients of pressure extending from the leading edge down which suggests intense vorticity in this region, i.e., similar to that observed in ABL flows.
- The pressure field corresponding to the time of maximum lift on the cube highlights illustrates that unlike the cube, there are stronger gradients of pressure over the roof for both the 0° and 90° yaw angles. There is also evidence of a slight asymmetry although this is less apparent in the animated distributions (www.birmingham.ac.uk/transient-winds).

## Acknowledgements

The authors would like to express their gratitude to the ESPRC for their support for this research through grant number EP/J008281/1. They would also like to thank Mike Vanderstam for his assistance in building and maintaining the transient wind simulator.

## References

Butler, K., Cao, S., Kareem, A., Tamura, Y., Ozono, S., 2010. Surface pressure and wind load characteristics on prisms immersed in a simulated transient gust front flow field. J. Wind Eng. Ind. Aerodyn. 98, 299–316.

Butler, K., Kareem, A., 2007. Physical and numerical modeling of downburst generated gust fronts. In: Proceedings of the 12th International Conference on Wind Engineering, Cairns, Australia, pp. 791–798.
Chang, C., 1971. Tornado effects on buildings and structures with laboratory simulation. In: Proceedings of 3rd International Conference on Wind Effects on Buildings and Structures, Tokyo, Japan, pp. 151–174.
Chay, M.T., Albermani, F., Wilson, R., 2006. Numerical and analytical simulation of downburst wind loads. Eng. Struct. 28, 240–254.
Chay, M.T., Letchford, C.W., 2002a. Pressure distributions on a cube in a simulated thunderstorm downburst – Part A: stationary downburst observations. J. Wind Eng. Ind. Aerodyn. 90, 711–732.
Chay, M.T., Letchford, C.W., 2002b. Pressure distributions on a cube in a simulated thunderstorm downburst – Part B: moving downburst observations. J. Wind Eng. Ind. Aerodyn. 90, 733–753.
Choi, E.C.C., 2004. Field measurement and experimental study of wind speed profile during thunderstorms. J. Wind Eng. Ind. Aerodyn. 92, 275–290.
Fujita, T.T., 1985. Downburst: Microburst and Macroburst. University of Chicago Press, Chicago, Illinois.
Fujita, T.T., Wakimoto, R.M., 1981. Five scales of airflow associated with a series of downbursts on 16 July 1980. Mon. Weather Rev. 109, 1439–1456.
Gast, K.D., Schroeder, J.L., 2003. Supercell rear-flank downdraft as sampled in the 2002 thunderstorm outflow experiment. In: Proceedings of the 11th International Conference on Wind Engineering, ICWEIA, pp. 2233–2240.
Haan Jr, F.L., Sarkar, P.P., Gallus, W.A., 2008. Design, construction and performance of a large tornado simulator for wind engineering applications. Eng. Struct. 30, 1146–1159.
Haines, M., Sterling, M., Quinn, A., 2013. Interference effects around two model high rise buildings in a simulated non-synoptic event. In: Proceedings of the European-African Conference on Wind Engineering.
Hjelmfelt, M.R., 1988. Structure and life cycle of microburst outflows observed in Colorado. J. Appl. Meteorol. 27, 900–927.
Holmes, J.D., Hangan, H.M., Schroeder, J.L., Letchford, C.W., Orwig, K.D., 2008. A forensic study of the Lubbock-Reese downdraft of 2002. Wind Struct. 11, 137–152.
Holmes, J.D., Oliver, S.E., 2000. An empirical model of a downburst. Eng. Struct. 22, 1167–1172.
Jesson, M., Haines, M., Singh, N., Sterling, M., Taylor, I., 2013. Numerical and physical simulation of a thunderstorm downburst. In: Iyer, N.R., Krishna, P., Rajan, S.S., Harikrishna, P. (Eds.), Proceedings of the Eighth Asia-Pacific Conference on Wind Engineering. Research Publishing, Chennai, India, pp. 561–564.
Jischke, M., Light, B., 1983. Laboratory simulation of tornadic wind loads on a rectangular model structure. J. Wind Eng. Ind. Aerodyn. 13, 371–382.
Kim, J., Hangan, H., 2007. Numerical simulations of impinging jets with application to downbursts. J. Wind Eng. Ind. Aerodyn. 95, 279–298.
Lin, W.E., 2010. Validation of a Novel Downdraft Outflow Simulator: A Slot Jet Wind Tunnel. The School of Graduate and Postdoctoral Studies. The University of Western Ontario, Ontario.
Lin, W.E., Orf, L.G., Savory, E., Novacco, C., 2007. Proposed large-scale modelling of the transient features of a downburst outflow. Wind Struct. 10, 315–346.
Lombardo, F.T., 2011. Thunderstorm Characteristics of Wind Engineering Importance. National Institute of Standards and Technology, Gaithersberg, MD.
Lundgren, T.S., Yao, J., Masour, N.N., 1992. Microburst modelling and scaling. J. Fluid Mech. 239, 461–488.
Mallipudi, S.V., Selig, M., Long, K., 2004. Use of a four-hole cobra pressure probe to determine the unsteady wake characteristics of rotating objects. In: Proceedings of the 24th AIAA Aerodynamic Measurement Technology and Ground Testing Conference. American Institute of Aeronautics and Astronautics, Inc.
Mason, M.S., 2003. Pulsed Jet Simulation of Thunderstorm Downbursts. Civil Engineering. Texas Tech University.
Mason, M.S., James, D.L., Letchford, C.W., 2009a. Wind pressure measurements on a cube subjected to pulsed impinging jet flow. Wind Struct. 12, 77–88.
Mason, M.S., Wood, G.S., Fletcher, D.F., 2009b. Numerical simulation of downburst winds. J. Wind Eng. Ind. Aerodyn. 97, 523–539.
McConville, A.C., 2008. The Physical Simulation of Thunderstorm Downbursts. School of Civil Engineering, University of Birmingham, Birmingham, UK.
McConville, A.C., Sterling, M., Baker, C.J., 2009. The physical simulation of thunderstorm downbursts using an impinging jet. Wind Struct. 12, 133–149.
Mehta, K.C., Levitan, M.L., Iverson, R.E., McDonald, J.R., 1992. Roof corner pressures measured in the field on a low building. J. Wind Eng. Ind. Aerodyn. 41, 181–192.
Mishra, A.R., James, D.L., Letchford, C.W., 2008. Physical simulation of a single-celled tornado-like vortex, Part A: Flow field characterization. J. Wind Eng. Ind. Aerodyn. 96, 1243–1257.
Orwig, K.D., Schroeder, J.L., 2007. Near-surface wind characteristics of extreme thunderstorm outflows. J. Wind Eng. Ind. Aerodyn. 95, 565–584.
Richards, P.J., Hoxey, R.P., Short, L.J., 2001. Wind pressures on a 6 m cube. J. Wind Eng. Ind. Aerodyn. 89, 1553–1564.
Sengupta, A., Haan, F.L., Sarkar, P.P., Balaramudu, V., 2008. Transient loads on buildings in microburst and tornado winds. J. Wind Eng. Ind. Aerodyn. 96, 2173–2187.
SensorTechnics, 2014. HCLA Series Miniature Amplified Low Pressure Sensors Datasheet. SensorTechnics.
Sohankar, A., 2006. Flow over a bluff body from moderate to high Reynolds numbers using large eddy simulation. Comput. Fluids 35, 1154–1168.
Sterling, M., Baker, C.J., Haines, M., Quinn, A.D., 2011. Scaling a thunderstorm downburst simulator, 13th International Conference on Wind Engineering. ICWE, RAI, Amsterdam, The Netherlands.
Vermeire, B.C., Orf, L.G., Savory, E., 2011. Improved modelling of downburst outflows for wind engineering applications using a cooling source approach. J. Wind Eng. Ind. Aerodyn. 99, 801–814.
Wang, L., Kareem, A., 2004. Modeling of non-stationary winds in gust-fronts. In: Proceedings of the 9th ASCE Specialty Conference on Probabilistic Mechanics and Structural Reliability.
Wang, L., McCullough, M., Kareem, A., 2013. A data-driven approach for simulation of full-scale downburst wind speeds. J. Wind Eng. Ind. Aerodyn. 123 (Part A), 171–190.
Wood, G.A., Kwok, K.C.S., Motteram, N.A., Fletcher, D.A., 2001. Physical and numerical modelling of thunderstorm downbursts. J. Wind Eng. Ind. Aerodyn. 89, 535–552.
Zhang, Y., Sarkar, P., Hu, H., 2013. An experimental study of flow fields and wind loads on gable-roof building models in microburst-like wind. Exp. Fluids 54, 1–21.